J. Fluid Mech. (1976), *vol.* 78, *part* 1, *pp.* 65–85
Printed in Great Britain

Transient combined laminar free convection and radiation in a rectangular enclosure

By D. W. LARSON
Sandia Laboratories, Albuquerque, New Mexico 87115
AND R. VISKANTA
Purdue University, West Lafayette, Indiana 47907

(Received 1 February 1974 and in revised form 28 June 1976)

The mass, momentum and energy-transfer equations are solved to determine the response of a rectangular enclosure to a fire or other high-temperature heat source. The effects of non-participating radiation, wall heat conduction, and laminar natural convection are examined. The results indicate that radiation dominates the heat transfer in the enclosure and alters the convective flow patterns significantly. At a dimensionless time of 5·0 the surface of the wall opposite a vertical heated wall has achieved over 99 % of the hot-wall temperature when radiation is included but has yet to change from the initial temperature for pure convection in the enclosure. At the same time the air at the centre of the enclosure achieves 33 % and 13 % of the hot-wall temperature with and without radiation, respectively. For a hot upper wall the convection velocities are not only opposite in direction but an order of magnitude larger when radiation transfer between the walls is included.

1. Introduction

In the last two decades efforts have been made to gain an understanding of the hostile free-burning fire in an attempt to achieve more effective methods of detection and control. One of the many individual problems which must be solved to obtain a more complete knowledge of the total problem of fires and fire spread in buildings is that of understanding and predicting the processes by which heat is transferred from a fire to the surrounding enclosure. In an attempt to gain some of the insight into the problem needed, an analysis was conducted of the mass, momentum and energy transfer which occurs in an enclosure owing to the presence of a high-temperature heat source.

There has been considerable research interest in the internal flow problem of enclosed natural convection in recent years, derived from such diverse applications as double-glazed windows, gaseous-core nuclear reactors, spent-fuel shipping casks, cryogenic liquid storage and enclosed fires. A review of most of the early theoretical and experimental investigations is given by Elder (1965) and in the review article by Ostrach (1972). One of the first successful attempts at a numerical solution of a natural convection problem was conducted by Hellums & Churchill (1961). They developed an explicit transient finite-difference method

and obtained transient and steady-state solutions to the problem of natural convection on an isothermal vertical surface, for which an exact solution exists, and also for natural convection in a long horizontal cylinder with one vertical end heated and the other cooled. Wilkes & Churchill (1966) extended the method of solution developed by Hellums & Churchill to analyse the problem of convection in a rectangular enclosure. However, they experienced instabilities which prevented them from obtaining solutions for Grashof numbers greater than 10^5. The instabilities were attributed to the fact that the old boundary vorticities were assumed to be valid during the computation of the new interior vorticities over a time step. Numerous other investigators have studied similar internal free-convection problems for various geometries and parameter ranges. A few of particular interest include the work of Aziz & Hellums (1967), who first reported results on three-dimensional natural convection in a cubical cavity. Davis (1968) and Rubel & Landis (1969) formulated the enclosed rectangular-cavity problem in terms of a nonlinear fourth-order equation for the stream function without the explicit appearance of vorticity in an attempt to avoid the numerical instabilities encountered by Wilkes & Churchill (1966). The iterative solution method yielded steady-state results. Davis reported no numerical difficulties for Rayleigh numbers as large as 2×10^5; however, Rubel & Landis encountered, at only slightly higher Rayleigh numbers ($Ra = 2{\cdot}4 \times 10^5$ for $Pr = 1$ and $Ra = 3{\cdot}6 \times 10^5$ for $Pr = 6$), the difficulty experienced by Wilkes & Churchill of physically impossible local temperature peaks. Chen (1971) demonstrated that the instabilities experienced by Wilkes & Churchill and others were not caused by the conjectured boundary vorticity lag. He also showed that anomalies in the temperature profile predicted at high Grashof number could be eliminated by finer spatial discretization. Torrance, Orloff & Rockett (1969) performed an experimental study of natural convection in cylindrical and rectangular enclosures and Torrance & Rocket (1969) conducted a corresponding numerical analysis of the cylindrical enclosure. This appears to be the earliest work where Grashof numbers greater than 10^6 were considered. In a separate paper, Torrance (1968) compared several finite-difference techniques which had been developed for the prediction of natural convection flows and pointed out that the finite-difference forms of the equations used by most previous investigators do not conserve energy or vorticity as do the original differential equations. Finally, Newell & Schmidt (1970) examined the problem of laminar natural convection in an enclosure over a range of parameters sufficient to determine a power-law correlation of the Nusselt number as a function of the Grashof number and aspect ratio. However, they used a non-conservative finite-difference scheme and were not able to obtain solutions for Grashof numbers greater than 10^5. A more complete survey and a more detailed discussion of these and other works can be found in Larson (1972). A thorough discussion of various numerical methods can be found in the book by Roache (1972). Recent related work includes that by Greenspan & Schultz (1974), Ozoe, Sayama & Churchill (1974, 1975), Peckover & Hutchinson (1974), and Cormack, Leal & Seinfeld (1974).

The work to date on natural convection in enclosures invariably includes temperature-specified and/or adiabatic wall boundary conditions. In addition,

certain of the solution techniques determine only the steady-state results. Neither of these conditions is appropriate for certain classes of problems, in particular the enclosed-fire or heat-source problems. For an enclosed fire the transient development of the flow patterns and the transient heat flow is of great interest. In addition, the thermal response of finite-thickness and finite-heat-capacity conducting walls is of interest since it would, for example, determine the rate of fire spread. Finally, the radiant heat transfer occurring in the enclosure and its influence upon the flow patterns and heat transfer have not previously been considered. In this paper the transient response of a rectangular enclosure to a specified high-temperature heat source is studied, including the effects of radiation, wall heat conduction, and laminar natural convection.

2. Analysis

Physical model

The model used for this study is illustrated in figure 1. The two-dimensional rectangular enclosure is surrounded by walls of uniform thickness. Initially, the enclosed air and walls are at some uniform temperature and the air is stagnant. At time $t > 0$ a specified high-temperature heat source is presumed to exist in some arbitrary (specified) part of the enclosure. For this analysis the air is confined to the enclosure and assumed to be radiatively non-participating. The basic assumptions made in the analysis are as follows.

(i) The fluid motion and heat-transfer processes are two-dimensional.

(ii) The fluid is Newtonian, compressibility is negligible, and the flow is laminar.

(iii) Viscous heat dissipation is negligible in comparison with conduction and convection.

(iv) All physical properties are constant except for the density, whose variation with temperature is allowed for in the buoyancy term.

(v) The walls are grey diffuse emitters and reflectors of radiation.

(vi) The Boussinesq approximation is valid.

The validity of the first two assumptions can be questioned for fire simulation, first because the size of most enclosures where fires occur is such that three-dimensional effects will be present and second because fully developed fires are highly turbulent. There are, however, other enclosed natural convection problems where these assumptions are realistic. In addition, considerable insight into the flow phenomena and heat transfer of the problem can be gained initially without introducing the considerable complexity of turbulent three-dimensional motion. Furthermore, the two-dimensional geometry lends itself most readily to rigorous formulation and the solution of radiative transfer so that these effects can be examined. The third assumption is readily justifiable in natural convection flows. The assumption of constant (temperature-independent) physical properties is primarily a numerical convenience and is frequently adopted in generalized analyses in order to decrease the number of independent parameters. In dimensionless form the parameters of the governing conservation equations frequently have a much weaker temperature dependence than do the physical

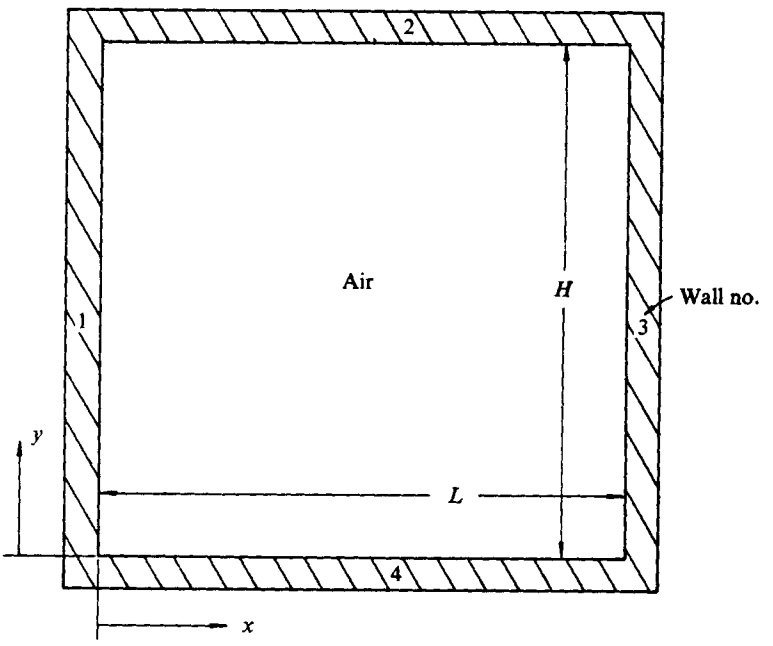

FIGURE 1. Physical model of enclosure.

properties. Toor & Viskanta (1972) have shown that for most enclosures the assumption of grey diffuse walls is a reasonable approximation to reality. The Boussinesq approximation accounts for the density variation in the buoyancy term, but neglects it in the inertial terms of the equations of motion, consistent with the assumptions of constant physical properties. This approximation also implies that, in the momentum equation, $\beta(T-T_m)$ is small relative to unity, where β is the thermal expansion coefficient, T is the local temperature and T_m is the mean temperature in the enclosure. The approximation is least correct for high-Grashof-number situations, early in the transient response particularly, when the temperature differences in the enclosure are large. However, Torrance & Rockett (1969) obtained good agreement with experimental results even when the Boussinesq condition was not satisfied.

Governing equations

The governing equations include the conservation equations of mass, momentum and energy and the radiative-transfer equations in an enclosure. The continuity and momentum equations can be transformed to stream-function and vorticity equations by cross-differentiation and combining momentum equations to eliminate the pressure term and introducing a stream function which automatically satisfies continuity. For the conditions described previously, the equations can be expressed in non-dimensional form by introducing the dimensionless variables $U = u/u_0$, $V = v/u_0$, $\theta = T/T_H$, $X = x/L$, $Y = y/L$, $\tau = tu_0/L$, $\Omega = \omega L/u_0$, $\Psi = \psi/u_0 L$, where $u_0 = (g\beta\Delta TL)^{\frac{1}{2}}$, u is the horizontal velocity, v the vertical velocity, T_H the maximum (source) temperature in the

enclosure, t the time, ω the vorticity, ψ the stream function, and ΔT the maximum initial temperature in the enclosure. As a result we obtain the following set of equations; the equations are referred to as the dimensionless energy equation

$$\frac{\partial\theta}{\partial\tau}+\frac{\partial(U\theta)}{\partial X}+\frac{\partial(V\theta)}{\partial Y}=\frac{1}{Pr(Gr)^{\frac{1}{2}}}\left(\frac{\partial^2\theta}{\partial X^2}+\frac{\partial^2\theta}{\partial Y^2}\right), \tag{1}$$

where Pr is the Prandtl number ν/α and Gr is the Grashof number $g\beta\Delta TL^3/\nu^2$, the dimensionless vorticity-transport equation

$$\frac{\partial\Omega}{\partial\tau}+\frac{\partial(U\Omega)}{\partial X}+\frac{\partial(V\Omega)}{\partial Y}=\frac{1}{(Gr)^{\frac{1}{2}}}\left(\frac{\partial^2\Omega}{\partial X^2}+\frac{\partial^2\Omega}{\partial Y^2}\right)+\frac{T_H}{\Delta T}\frac{\partial\theta}{\partial X}, \tag{2}$$

the dimensionless velocity equations

$$U=\partial\Psi/\partial Y, \quad V=-\partial\Psi/\partial X, \tag{3a, b}$$

and the dimensionless stream-function equation

$$\Omega=-(\partial^2\Psi/\partial X^2+\partial^2\Psi/\partial Y^2). \tag{4}$$

The initial conditions in the enclosure are a specified uniform temperature and a stagnant gas. The boundary conditions are a specified temperature source in some part of the enclosure, no slip at the walls, and a zero value of the stream function at the walls. The boundary condition on vorticity is not known explicitly, but this presents no particular difficulty as noted later. An energy balance at the wall yields the condition

$$-\partial\theta_a/\partial\zeta=-N_k\,\partial\theta_w/\partial\zeta+N_r Q_r, \tag{5}$$

where ζ represents the dimensionless co-ordinate normal to the wall, N_k is the thermal conductivity ratio k_w/k_a, N_r is the dimensionless radiation-to-conduction parameter $\sigma T_H^3 L/k_a$, $Q_r=q_r/\sigma T_H^4$ and σ is the Stefan–Boltzmann constant. It is this boundary condition which couples the radiative, convective and conductive heat transfer in the problem. Any change in wall surface temperature simultaneously affects the convection to the wall, the conduction inside the wall, and the net radiant heat flux at the wall.

The above dimensionless equations are in slightly different forms from those developed and used by previous investigators of natural convection in enclosures. There are two reasons for the differences. Since there is no characteristic velocity under natural convection conditions there is no unique way of defining a dimensionless velocity. Instead, a reference velocity must be selected from examination of the physical problem and a consideration of the controlling forces. Previous investigators have typically selected a characteristic velocity related to the viscous forces, $u_0=\nu/L$. It appears, however, that a more meaningful dimensionless parameter may result, in a buoyancy-dominated situation, by relating the characteristic velocity to the buoyancy forces, and thus the selection $u_0^2=g\beta\Delta TL$ was made. The second reason for the differences results from the definition of dimensionless temperature. In purely convective (or conductive) heat-transfer situations, it is convenient to define the dimensionless temperature as the ratio of temperature differences, and all previous analyses have done so. However, when radiation is also present such a definition is inappropriate since the driving

potential for heat transfer is no longer a linear temperature difference. Therefore, because of the radiative–convective coupling, the dimensionless temperature is defined here as a temperature ratio.

3. Radiative heat transfer

The equations for radiative heat transfer in an enclosure in local thermodynamic equilibrium are given for grey diffuse walls with an arbitrary temperature distribution. The radiative flux along wall i is given by

$$q_{ri}(s_i) = (\epsilon_i/\rho_i)\,[\sigma T_i^4(s_i) - J_i(s_i)], \tag{6}$$

where s_i represents a position on wall i, ϵ_i and ρ_i are the emissivity and reflectivity, respectively, of wall i, and the radiosity $J_i(s_i)$ for plane walls is given by (Sparrow & Cess 1966)

$$J_i(s_i) = \epsilon_i \sigma T_i^4(s_i) + \rho_i \sum_{\substack{j=1 \\ j \neq i}}^{m} \int_{Aj} J_j(s_j)\, K(s_i, s_j)\, dA_j. \tag{7}$$

The kernel $K(s_i, s_j)$ is a function of the configuration. For the geometry of figure 1, (7) can be evaluated for each wall to yield

$$J_1(y_1) = \epsilon_1 \sigma T_1^4(y_1) + \frac{\rho_1}{2}\left\{\int_0^L \frac{J_2(x_2)\,(H-y_1)\,x_2}{[(H-y_1)^2+x_2^2]^{\frac{3}{2}}}\,dx_2 + \int_0^H \frac{J_3(y_3)\,L^2}{[L^2+(y_3-y_1)^2]^{\frac{3}{2}}}\,dy_3 + \int_0^L \frac{J_4(x_4)\,y_1\,x_4}{[y_1^2+x_4^2]^{\frac{3}{2}}}\,dx_4\right\}, \tag{8a}$$

$$J_2(x_2) = \epsilon_2 \sigma T_2^4(x_2) + \frac{\rho_2}{2}\left\{\int_0^H \frac{J_1(y_1)\,x_2(H-y_1)}{[x_2^2+(H-y_1)^2]^{\frac{3}{2}}}\,dy_1 + \int_0^H \frac{J_3(y_3)\,(H-y_3)\,(L-x_2)}{[(H-y_3)^2+(L-x_2)^2]^{\frac{3}{2}}}\,dy_3 + \int_0^L \frac{J_4(x_4)\,H^2}{[H^2+(x_4-x_2)^2]^{\frac{3}{2}}}\,dx_4\right\}, \tag{8b}$$

$$J_3(y_3) = \epsilon_3 \sigma T_3^4(y_3) + \frac{\rho_3}{2}\left\{\int_0^H \frac{J_1(y_1)\,L^2}{[L^2+(y_1-y_3)^2]^{\frac{3}{2}}}\,dy_1 + \int_0^L \frac{J_2(x_2)\,(H-y_3)\,(L-x_2)}{[(H-y_3)^2+(L-x_2)^2]^{\frac{3}{2}}}\,dx_2 + \int_0^L \frac{J_4(x_4)\,y_3(L-x_4)}{[y_3^2+(L-x_4)^2]^{\frac{3}{2}}}\,dx_4\right\}, \tag{8c}$$

$$J_4(x_4) = \epsilon_4 \sigma T_4^4(x_4) + \frac{\rho_4}{2}\left\{\int_0^H \frac{J_1(y_1)\,x_4 y_1}{[x_4^2+y_1^2]^{\frac{3}{2}}}\,dy_1 + \int_0^L \frac{J_2(x_2)\,H^2}{[H^2+(x_2-x_4)^2]^{\frac{3}{2}}}\,dx_2 + \int_0^H \frac{J_3(y_3)\,(L-x_4)\,y_3}{[y_3^2+(L-x_4)^2]^{\frac{3}{2}}}\,dy_3\right\}. \tag{8d}$$

Equations (6), (7) and (8) can readily be non-dimensionalized, but for brevity the results are not included here. As a practical consideration, however, it should be mentioned that in solving the radiosity equations the integral terms are evaluated in their dimensional form and then the result is non-dimensionalized. This procedure takes advantage of symmetry of the kernel which would not be possible for any $L/H \neq 1$ if the equations were non-dimensionalized before evaluation of the integrals.

4. Heat conduction in the wall

The heat conduction in the wall was assumed to be one-dimensional. This assumption is reasonable since the thermal conductivity of the non-metallic walls is generally quite low and the temperature gradient in the normal direction is considerably larger than along the plane of the wall. Therefore the dimensionless energy equation in the wall can be written as

$$\partial\theta/\partial\tau = N_\alpha N_L^{-2} Pr^{-1} Gr^{-\frac{1}{2}} \partial^2\theta/\partial\zeta^2, \tag{9}$$

where N_α is α_w/α_a, the ratio of the wall thermal diffusivity to the air thermal diffusivity, and $N_L = L_w/L$.

The external surface of the walls can either be insulated or have a specified convective-heat-transfer coefficient. Owing to the low conductivity of the walls the results for either condition are essentially the same; however, the results reported here assumed the horizontal walls to be externally insulated and the external vertical walls to have convective transfer to ambient temperature.

5. Method of solution

Equations (1)–(4) along with (6), (8), (9) and their appropriate initial and boundary conditions are sufficient to describe the problem completely. The equations are all coupled either through the variables or the boundary conditions or both. The conservation equations were solved using an alternating-direction implicit (A.D.I.) finite-difference scheme. The nonlinear convective terms were represented by an 'upstream' finite-difference form as suggested by Torrance (1968) for buoyancy-dominated flow.

The boundary condition on the internal wall surface must be given careful consideration so that the heat flux conducted into the wall is equal to the net flux convected (conducted) and radiated to the wall surface. The energy equation is solved at the surface by expanding the dimensionless temperature in a Taylor series at that location which, ignoring third- and higher-order terms, yields for the second derivative along the vertical wall

$$\frac{\partial^2\theta_{0,w}}{\partial X^2} = \frac{2(\theta_{1,w} - \theta_{0,w})}{(\Delta X)^2} - \frac{2}{\Delta X}\frac{\partial\theta_{0,w}}{\partial X}, \tag{10}$$

where the nodal numbering system in the wall and in the enclosure is shown in figure 2. Now from the boundary condition (5), we have

$$\frac{\partial\theta_{0,w}}{\partial X} = N_k^{-1}\frac{\partial\theta_{0,a}}{\partial X} + N_r Q_r. \tag{11}$$

The radiative flux Q_r is known from the solution of the radiative-flux equation (6) which in turn is determined from a solution of the radiosity equations (8). In solving the integral radiosity equations (8*a–d*), the kernels of the equations were first evaluated and stored for the geometry of interest, taking advantage of symmetry to save storage and computing time. The equations were then solved by the method of successive approximation. The integrals were evaluated by

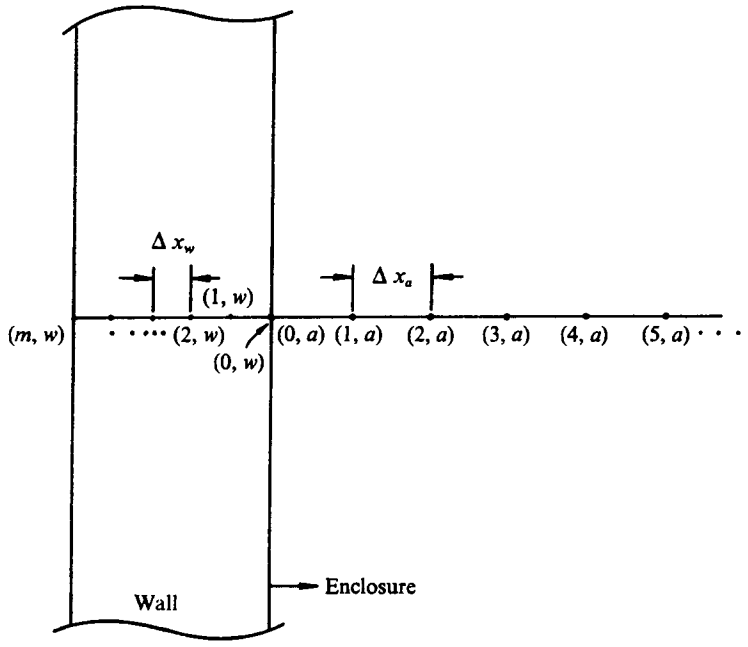

FIGURE 2. Representative nodal scheme in wall and enclosure for Taylor series expansion.

Simpson's rule. The temperature gradient in the air at the wall surface must be evaluated by forward differences. Using a cubic polynomial approximation to represent the temperature of the air near the wall and substituting (11) into (10), we obtain the finite-difference form of the second derivative of wall temperature at the surface which satisfies the interior boundary condition. The result is

$$\frac{\partial^2\theta_{0,w}}{\partial X^2} = \frac{2(\theta_{1,w}-\theta_{2,w})}{(\Delta X_w)^2} - \frac{2}{\Delta X_w}\frac{1}{N_K}\left[\frac{(-7\theta_{0,a}+8\theta_{1,a}-\theta_{2,a})}{6\Delta X_a} + N_r Q_r\right]. \tag{12}$$

Since the results indicate that the radiative term $N_r Q_r$ dominates the other terms in (12), the finite-difference form used to evaluate the temperature gradient in the air has very little effect.

Since the boundary conditions for the vorticity-transport equation are not known, it is necessary to determine the wall vorticities from additional considerations. Following Wilkes & Churchill (1966) this is accomplished by a Taylor series expansion of the stream function in the vicinity of the wall. By using the boundary conditions on Ψ and noting from the stream-function equation (4) that $\Omega_{0,j} = \partial^2\Psi/\partial X^2$, an approximation for vorticity at the new time step at the wall is obtained from the values of the interior stream function,

$$\Omega_{0,j} = -(8\Psi_{1,j}-\Psi_{2,j})/2(\Delta X)^2. \tag{13}$$

The stream-function equation (4) is an elliptic equation which is notoriously difficult and time consuming to solve by numerical methods. The method of successive over-relaxation (S.O.R.) has proved quite successful and has been adopted by the majority of the researchers. In a paper comparing finite-difference

techniques for natural convection, Torrance (1968) indicates that the solution of (4) is the most time-consuming portion of the problem, with one iterative sweep requiring as much time as the entire computation of the new temperature or vorticity field. For this problem a more efficient method of solving (4) was first suggested by Peaceman & Rachford (1955). The procedure is to rewrite the elliptic equation as a time-dependent equation,

$$\partial\Psi/\partial\tau = \partial^2\Psi/\partial X^2 + \partial^2\Psi/\partial Y^2 + \Omega. \tag{14}$$

This equation is now of the parabolic type and can be integrated in time by the previously described A.D.I. method until steady state is reached. Since only the steady value is of interest here the implicit procedure allows the use of large time steps, and convergence to steady state can be reached within a few iterations. Chen (1971) has demonstrated that, for a uniformly distributed error, 14 iterations of S.O.R. are required to reduce the error by a factor of 10^{-2} while the A.D.I. method requires 3 iterations to achieve the same error reduction. This improved convergence allows a considerable amount of time to be saved in the solution of the stream-function equation and thus permits also the use of an implicit scheme with large time steps in the solution of the energy and vorticity-transport equations. Roache (1972) discusses other implications of the various methods for solving the elliptic equation. The velocity equations are solved using four-point central-difference representations of (3*a* and *b*) at all nodal points more than one grid space away from the walls. The velocities at one grid space from the walls are obtained by a four-point non-central-difference form.

The solution procedure consisted of advancing the interior temperatures through a time step by solving (1). The vorticity-transport equation was then solved for all interior (non-boundary) nodal points. Next, the stream-function equation was solved. From the solution of the stream-function equation the wall (boundary) vorticities were updated and the velocity field at the new time step was determined. The radiation equations were then solved. From the temperature distribution in the enclosure, the convective flux to the walls was computed and added to the radiative flux. Finally, the temperature distribution in the walls was updated by solving the energy equation in the wall. The procedure was then repeated for a new time step. Allowance was made for iterating on the nonlinear terms during each time step; however, the results indicated that for reasonably sized time steps the iterative process was not required. Furthermore, in the problems involving radiation, the flow field changed much more slowly than did the temperature field and a considerable saving in computer time was obtained with no change in the results by solving the vorticity and stream-function equations (updating the flow field) every fifth time step.

A large number of numerical experiments were conducted in an effort to determine the time step, grid size, and convergence criteria which would lead to a reasonable compromise between accuracy and computing time. An internal check on the solution scheme was conducted by solving selected problems with both explicit and implicit finite-difference techniques and also by comparing limiting cases (temperature-specified boundaries and no radiative transfer) with earlier studies (Wilkes & Churchill 1966; Chen 1971). It was determined that for a square

enclosure ($L/H = 1{\cdot}0$) a 20×10 grid spacing (21×11 nodal points) was adequate to resolve the qualitative trends of fluid motion and temperature and also provide reasonable quantitative results for Grashof numbers of 10^6 or less. Grid spacings of 50×20 were necessary to prevent instabilities (local temperature peaks) from occurring up to $Gr = 10^9$, the upper limit of laminar flow. The detailed comparisons are given elsewhere (Larson 1972). The time step allowed was determined by numerical experiment to be controlled by the radiative heat transfer. Variable time steps were used since the wall surface temperature changed very rapidly early in the transient response but as the solution progressed smaller temperature changes allowed larger time steps. The effect of the time-step size was determined by halving the step until there was no noticeable change in the results. Typical run times for a 20×10 grid were less than 300 s for the full transient solution on a CDC 6600 computer.

6. Results and discussion

Parameters

The large number of variables governing the problem makes a thorough parametric study impractical without extensive amounts of computer time. Therefore the values selected for the parameters were determined as far as possible to be those characteristic of a typical room-size enclosure with some portion of the enclosure at the surface temperature of a flaming wall, albeit the Grashof number is artificially constrained to the laminar-flow regime for the results reported here. The influence of turbulent convection ($Gr > 10^9$) and radiatively participating combustion products was also examined and is reported in Larson (1972). The parameter values used in the simulations were $Gr = 10^5$–10^9, $Pr = 0{\cdot}73$, $N_k = 4{\cdot}0$, $N_\alpha = 0{\cdot}001$, $N_L = 0{\cdot}025$, $N_r = 2000$ and $\epsilon = 0{\cdot}6$–$0{\cdot}9$. In general, the results are for a square enclosure. Analytical simulations were conducted for numerous boundary conditions in the enclosure including a hot left wall, hot ceiling, hot floor, local hot spot on the ceiling, and local hot spot on the floor. Because of space limitations only a few of the results are presented here.

In order to make a rapid qualitative evaluation of the temperature field and flow field in the enclosure a computer program was written to plot the streamlines and isotherms on the line printer. The array being plotted is scanned for the range of values and then the range is divided into 10 subranges which are each assigned a specific print number (or blank). The resulting field of alternate numbers and blanks then shows 10 % bands of the array being plotted.

Simulation of hot left wall

The response of the enclosure to a hot left wall ($\theta = 1{\cdot}0$) with the room initially at $\theta = 0{\cdot}3$ was examined for a range of Grashof numbers from 10^5 to 10^9.

Figure 3 shows the streamlines caused by a hot left wall for a Grashof number of 10^5 at four different times with $\epsilon = 0{\cdot}9$. The streamlines develop relatively quickly although the initial velocities are very low. At $\tau = 2{\cdot}0$, a small anticlockwise eddy appears near the right wall owing to the buoyancy of the hot air near the wall. As time progresses the inertia of the large clockwise eddy moves

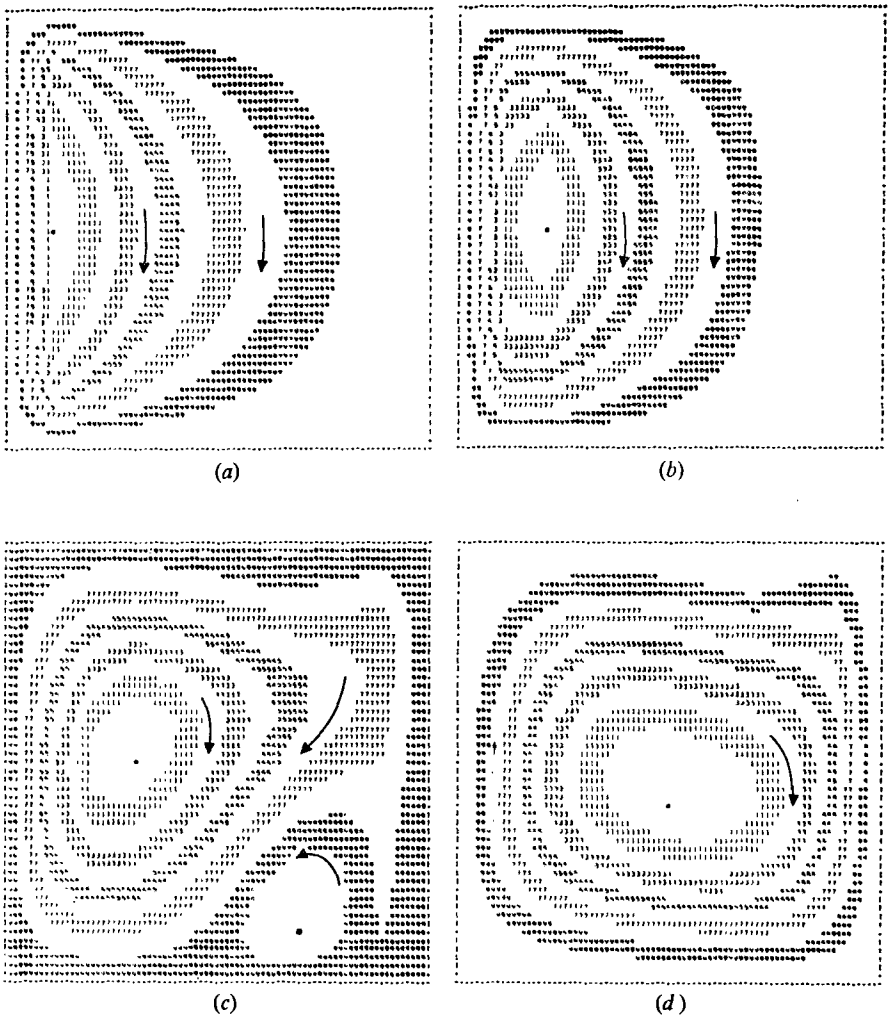

FIGURE 3. Streamlines in the enclosure for a hot left wall, $Gr = 10^5$, $\epsilon = 0{\cdot}9$. (*a*) $\tau = 0{\cdot}2$, (*b*) $\tau = 1{\cdot}0$, (*c*) $\tau = 5{\cdot}0$, (*d*) $\tau = 20{\cdot}0$.

the smaller eddy down the wall and compresses it. In the figure for $\tau = 5{\cdot}0$ the small eddy can be seen at the lower right-hand portion of the enclosure. A short time later the eddy is pulled off the wall and compressed near the floor and, by $\tau = 15{\cdot}0$, the eddy has disappeared into the main flow. Figure 4 illustrates the corresponding isotherms. Initially, the wall temperatures change rapidly owing to radiation, and the temperature of the air is increased by nearly pure conduction as evidenced by the linear variation of the isotherms near the walls. The influence of convection on the temperature profiles becomes clearly evident, however, by $\tau = 5{\cdot}0$ as shown by the downward bending of the isotherms near the centre-line. At $\tau = 20{\cdot}0$ the downward velocity on the right side of the enclosure deforms the isotherms significantly. Figure 5 depicts the development of the velocity profile with time at the mid-height of the enclosure. The velocity along the hot wall

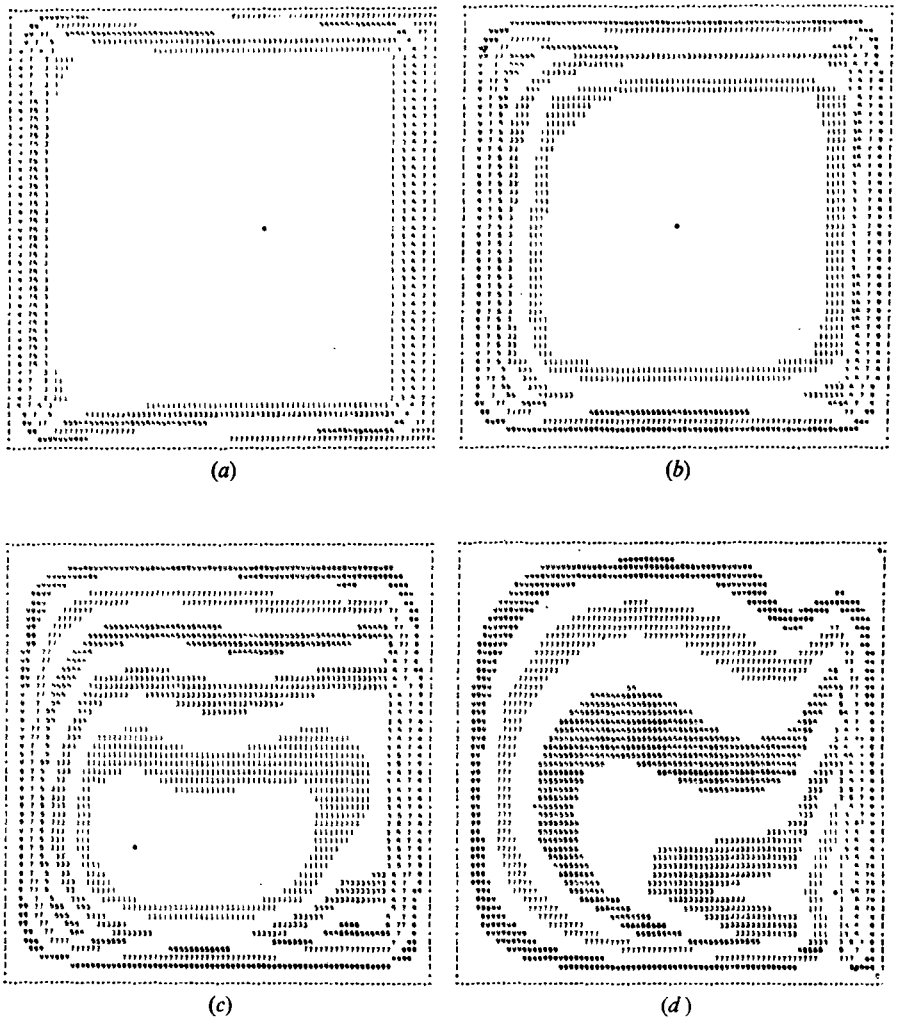

FIGURE 4. Isotherms in the enclosure for a hot left wall, $Gr = 10^5$, $\epsilon = 0{\cdot}9$. (a) $\tau = 0{\cdot}2$, (b) $\tau = 1{\cdot}0$, (c) $\tau = 5{\cdot}0$, (d) $\tau = 20{\cdot}0$.

develops quite rapidly and reaches a maximum before dropping back to a nearly steady value. This is caused by the time lag required for the cool air on the right wall to circulate and reach the hot surface on the left. The weak eddy that develops on the right wall appears as a small positive velocity near the right wall at $\tau = 1{\cdot}0$. The eddy also creates the local maximum at $x/L = 0{\cdot}8$ and $\tau = 3{\cdot}0$. At $\tau = 20{\cdot}0$ the velocity profile is very nearly symmetric about the centre-line of the enclosure. The temperature distribution at mid-height is shown in figure 6. The influence of the radiative transfer is very strong. The effect of the low-thermal-conductivity wall is such that the external surface of the wall has not experienced any temperature change even though the enclosure is approaching a uniform temperature. This result was typical of all the situations examined and thus the external surface boundary conditions had little influence on the results.

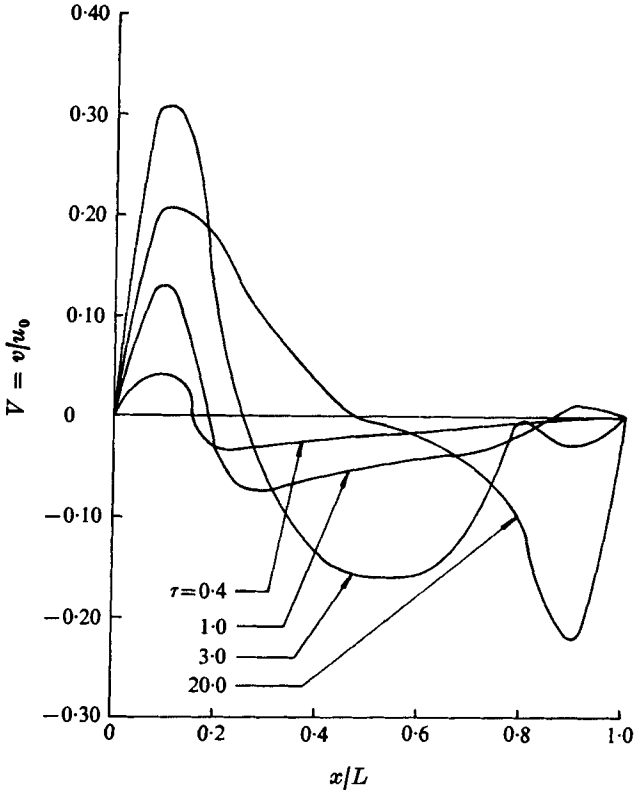

FIGURE 5. Velocity profile at enclosure mid-height ($y/H = 0{\cdot}5$), hot left wall, $Gr = 10^5$, $\epsilon = 0{\cdot}9$.

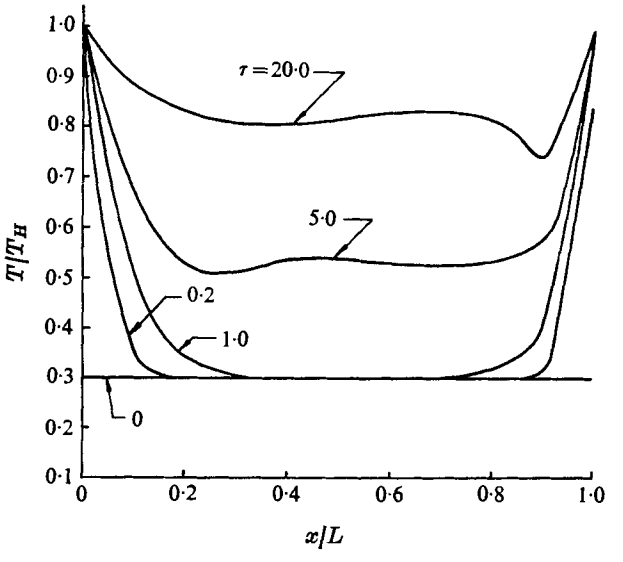

FIGURE 6. Temperature profile at enclosure mid-height ($y/H = 0{\cdot}5$), hot left wall, $Gr = 10^5$, $\epsilon = 0{\cdot}9$.

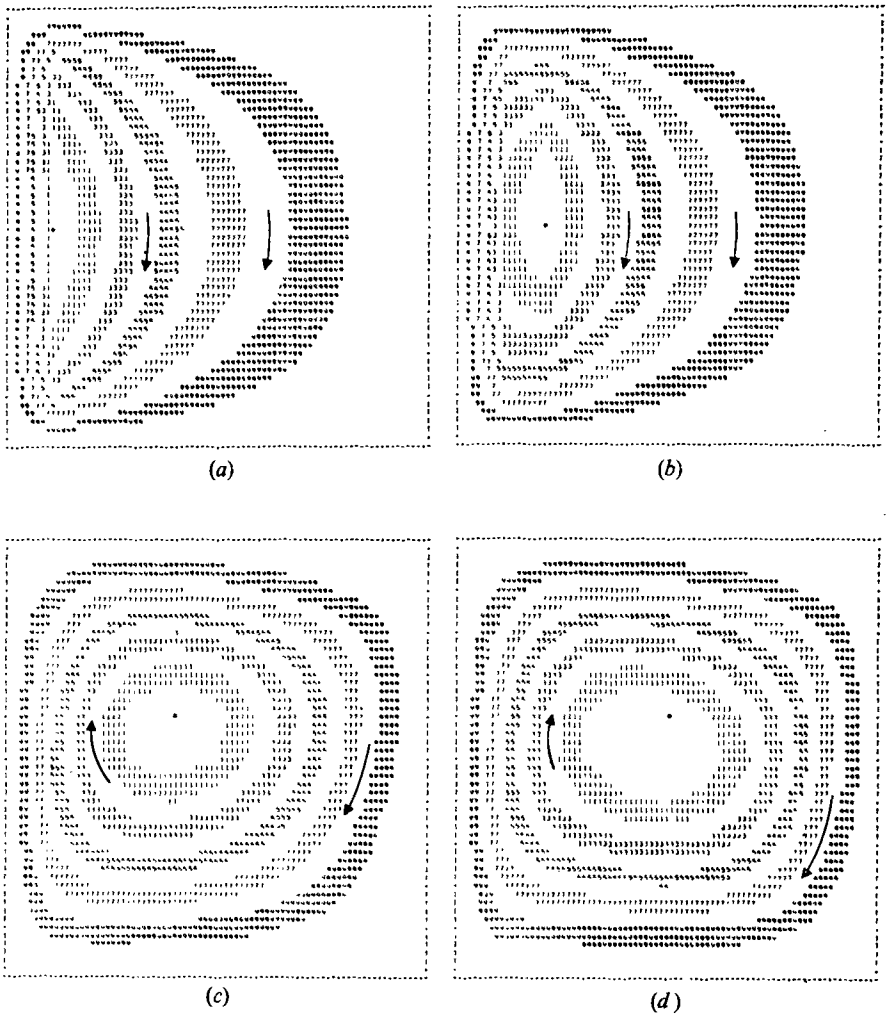

FIGURE 7. Streamlines in the enclosure for a hot left wall neglecting radiant heat transfer, $Gr = 10^5$. (a) $\tau = 0{\cdot}2$, (b) $\tau = 1{\cdot}0$, (c) $\tau = 5{\cdot}0$, (d) $\tau = 20{\cdot}0$.

The effect of radiation was determined by examining the same conditions while neglecting radiative transfer. The development of the streamlines, shown in figure 7, is very similar to those including radiation, the major difference being that no eddy appears on the right wall since there are no buoyancy forces there. The isotherms, however, are considerably changed. In figure 8 the influence of the moving air is first seen at $\tau = 1{\cdot}0$ as the isotherms begin to deflect slightly outwards near the ceiling, and, as convection develops, the isotherms continue to deform. Figures 9 and 10 show the velocity and temperature profiles, respectively, in the absence of radiative transfer. As seen in figure 10, the cool right wall is just beginning to feel the influence of the hot wall at $\tau = 20{\cdot}0$ when radiation is neglected.

Additional results were obtained for Grashof numbers of 10^6, 10^7 and 10^9

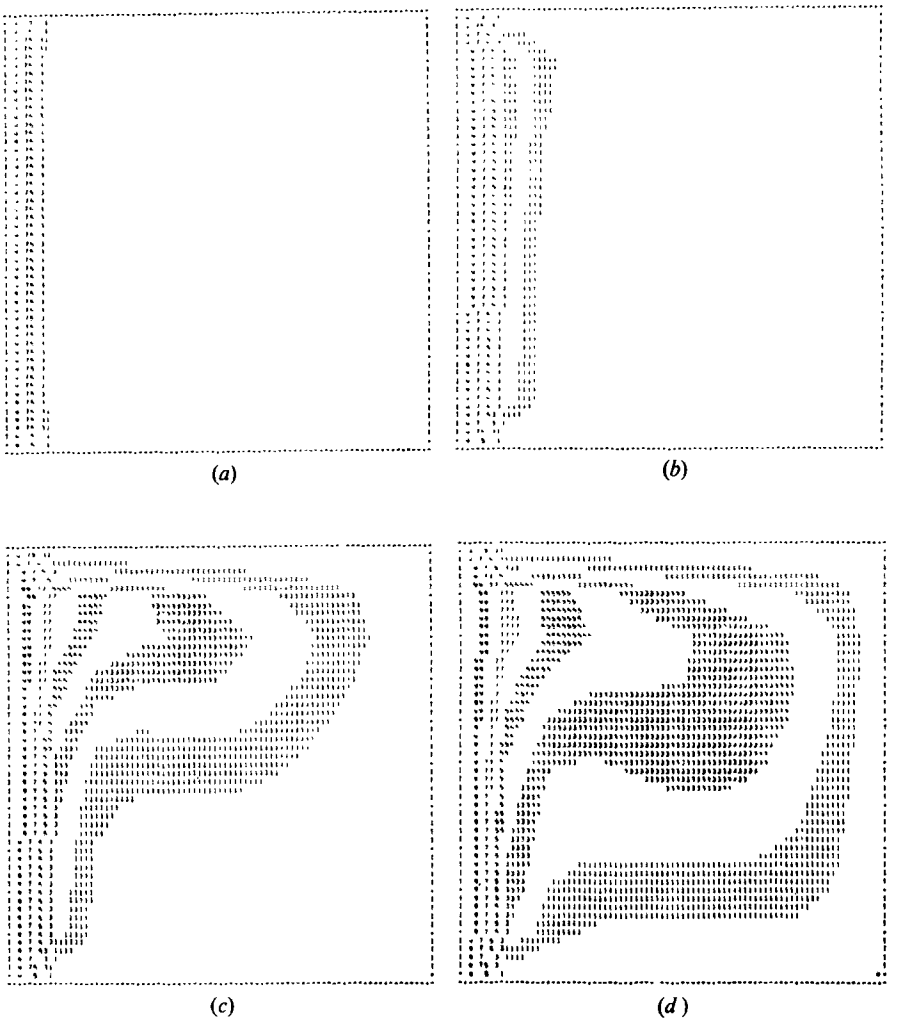

FIGURE 8. Isotherms in the enclosure for a hot left wall neglecting radiant heat transfer, $Gr = 10^5$. (*a*) $\tau = 0{\cdot}2$, (*b*) $\tau = 1{\cdot}0$, (*c*) $\tau = 5{\cdot}0$, (*d*) $\tau = 20{\cdot}0$.

(Larson 1972). The early development of the streamlines and isotherms was very similar. However, at the higher Grashof numbers the anti-clockwise eddy appearing on the right wall is considerably stronger and is able to maintain itself, resulting in irregularly shaped streamlines and isotherms at later times.

The influence of wall emissivity is shown in figure 11. The temperature distribution is shown along the ceiling at three different times for three different emissivity conditions in the enclosure. The hot wall emissivity was maintained at 0·9, and the cool wall emissivities were set at 0·9 or 0·6. In addition, the results of a semi-grey condition are also illustrated, where the emissivities are maintained at 0·9 but because the radiant energy from the hot wall is maximum around a wavelength of 3·0 μm, where some building materials have a lower absorptivity, the cool wall absorptivities are set equal to 0·6.

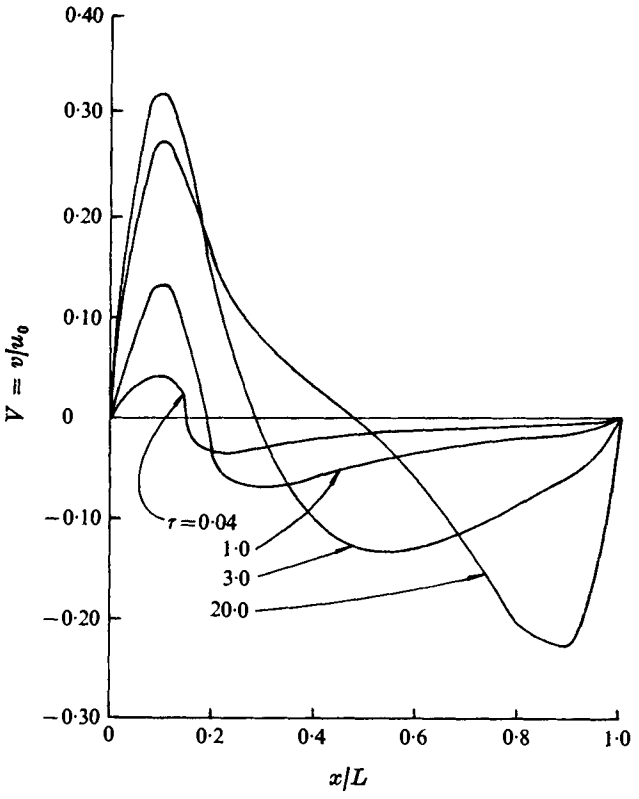

FIGURE 9. Velocity profile at enclosure mid-height ($y/H = 0{\cdot}5$) neglecting radiant heat transfer, hot left wall, $Gr = 10^5$.

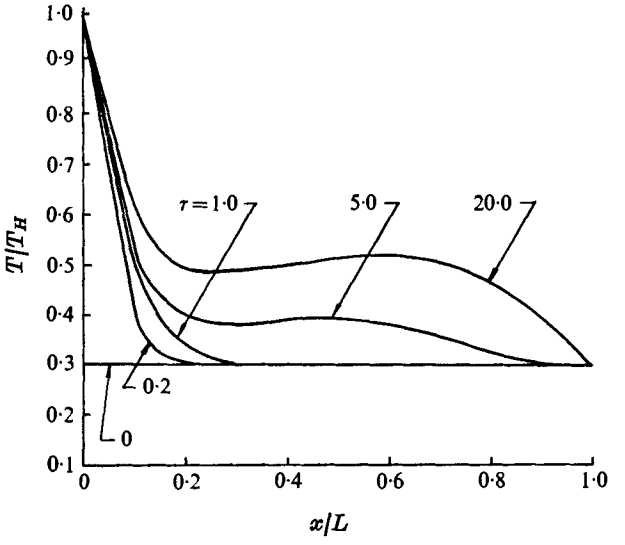

FIGURE 10. Temperature profile at enclosure mid-height ($y/H = 0{\cdot}5$) neglecting radiant heat transfer, hot left wall, $Gr = 10^5$.

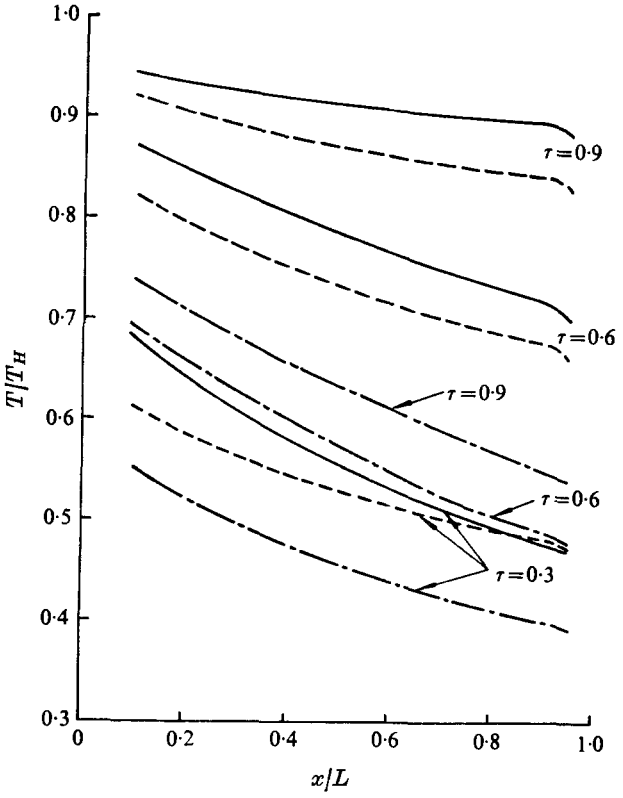

FIGURE 11. Temperature distribution on the ceiling for a hot left wall and three emissivity conditions, $Gr = 10^6$, $\epsilon_1 = 0·9$. —, $\epsilon_{2,3,4} = 0·9$; - - -, $\epsilon_{2,3,4} = 0·6$; -·-, semi-grey, $\epsilon = 0·9$, $\alpha_{2,3,4} = 0·6$.

It is interesting to note that early in the transient response ($\tau \leqslant 0·3$) the heat transfer to the right edge of the ceiling ($x/L \leqslant 0·8$) is increased rather than decreased by a decrease in emissivity. This result, surprising at first glance, is caused by the fact that lowering the cool wall emissivities also has the effect of raising their reflectivities. Since nearly all the net radiant energy is initially coming from the hot left wall, the increased reflectivity causes a more uniform distribution of radiant heat flux along the walls as evidenced by the smaller temperature drop across the enclosure. The net effect is an increase in heat transfer at the right edge of the ceiling. As the cool walls begin to heat up, the effect disappears owing to the increased heat transfer from all the walls.

The influence of the enclosure geometry was examined by a simulation with a hot left wall in an enclosure with an L/H value of 5·0. Even though the room is much longer, the flow pattern is very similar to that of the square enclosure, with two large eddy patterns developing, with the stronger eddy near the hot wall occupying approximately three-quarters of the enclosure (Larson 1972).

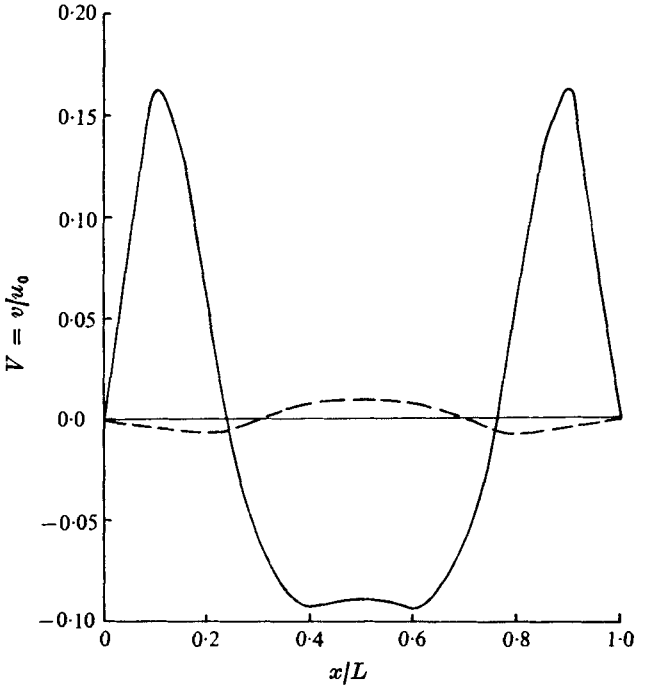

FIGURE 12. Velocity profile at enclosure mid-height ($y/H = 0{\cdot}5$) for a hot ceiling with and without radiant heat transfer, $\tau = 10$, $Gr = 10^6$, $\epsilon = 0{\cdot}9$. ——, with radiant heat transfer; – – –, without.

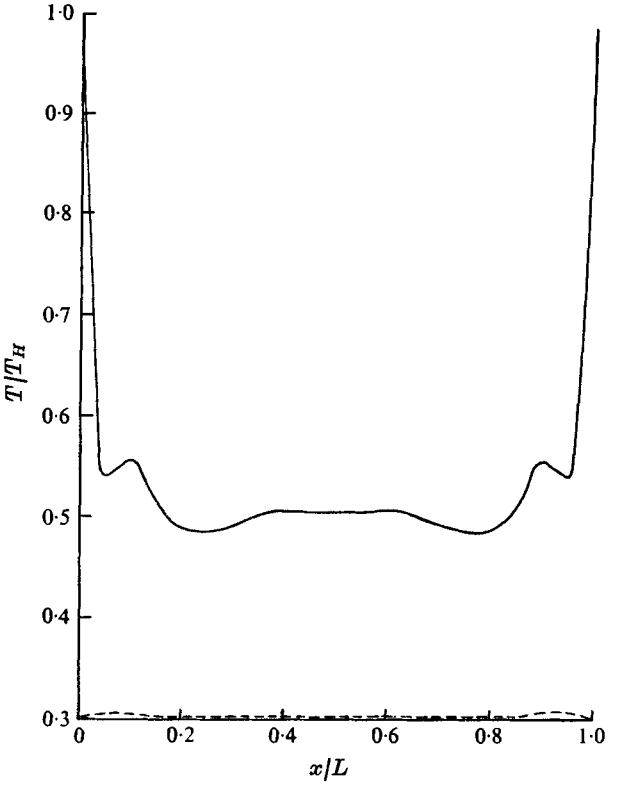

FIGURE 13. Temperature distribution at enclosure mid-height ($y/H = 0{\cdot}5$) for a hot ceiling with and without radiant heat transfer, $\tau = 10$, $Gr = 10^6$, $\epsilon = 0{\cdot}9$. ——, with radiant heat transfer; – – –, without.

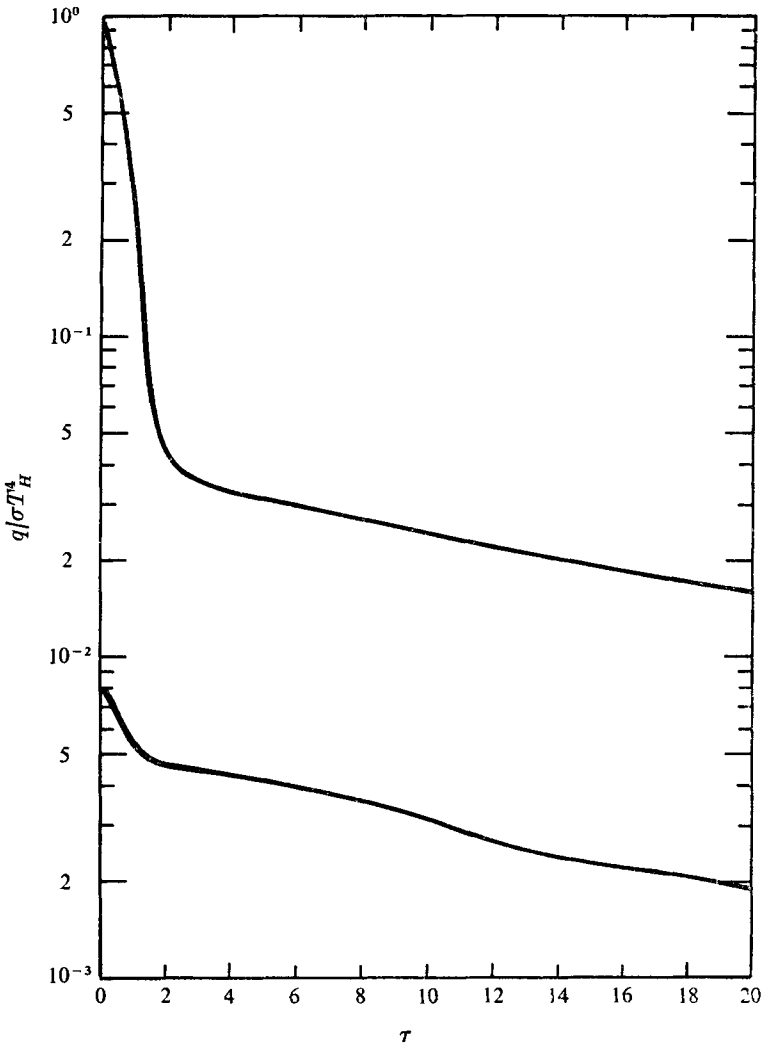

FIGURE 14. Net heat flux from hot left wall at $y/H = 0{\cdot}5$, $Gr = 10^6$, $\epsilon = 0{\cdot}9$. The upper curve is for radiant heat flux and the lower for convective heat flux.

Hot ceiling and hot floor

The effects of a ceiling fire were examined by assuming the surface of wall 2 (upper wall) to be hot ($\theta = 1{\cdot}0$) and the other wall surfaces to be initially at room temperature ($\theta = 0{\cdot}3$) for a square enclosure and a Grashof number of 10^6. The influence of the radiative heat transfer was very large, as indicated in figure 12. The radiative transfer induces much stronger convective currents which are, in fact, opposite in direction to those induced by convection alone. As a result the temperature distribution in the enclosure is altered considerably as shown in figure 13. The effect of a local hot spot centred on the upper surface produced similar results.

The effects of a floor fire were also examined. With the entire floor heated, the

development of the streamlines and temperature profiles were very similar to those for a hot ceiling. The influence of radiation was again very pronounced with the temperature everywhere within the enclosure increasing much more rapidly when radiation was included.

7. Heat transfer

A general correlation of the heat-transfer results is not possible owing to the complex interactions of the temperature and flow fields in the enclosure. Only a few of the many possible conditions that could exist have been examined; however, it appears that there is no *a priori* method which can predict the radiative, convective and total heat transfer without solving the entire problem. Figure 14 compares the radiative and convective heat flux from the midpoint of the hot left wall as a function of time. The rapid thermal response of the wall surfaces causes the radiative heat transfer to decrease sharply to a point where it is approximately a factor of ten larger than the convective transfer. In general, for the conditions examined, the radiative heat transfer was one or two orders of magnitude larger than the convective transfer and was essentially solely responsible for the temperature rise of the walls surrounding the heat source. This implies that fire spread in enclosures is primarily dominated by radiative transfer. Therefore, attempts to predict the thermal response and enclosed fluid-flow behaviour caused by a fire or other high temperature heat source requires the inclusion of radiation heat transfer if reasonable results are to be obtained.

8. Conclusions

When portions of an enclosure are at temperatures associated with fires, radiation is the predominant mechanism of heat transfer. The convective currents are significantly altered by the radiative heat transfer, frequently causing changes in both magnitude and direction. Simulation of a fire or other high temperature heat source in an enclosure therefore requires that radiation be included. The study also demonstrates that reasonably straightforward analytical and numerical techniques can be used to model the behaviour of complex natural phenomena.

This work was supported by the United States Energy Research and Development Administration.

REFERENCES

Aziz, K. & Hellums, J. D. 1967 Numerical solution of the three dimensional equations of motion for laminar natural convection. *Phys. Fluids*, **10**, 314.

Chen, T. S. 1971 A three-dimensional steady state mathematical model of a glass furnace. Ph.D. thesis, Purdue University.

Cormack, D. E., Leal, L. G. & Seinfeld, J. H. 1974 Natural convection in a shallow cavity with differentially heated end walls. Part 2. Numerical solutions. *J. Fluid Mech.* **65**, 231.

DAVIS, G. DEVAHL 1968 Laminar natural convection in enclosed rectangular cavity. *Int. J. Heat Mass Transfer*, **11**, 1675.

ELDER, J. W. 1965 Laminar free convection in a vertical slot. *J. Fluid Mech.* **23**, 77.

GREENSPAN, D. & SCHULTZ, D. 1974 Natural convection in an enclosure with localized heating from below. *Comp. Methods Appl. Mech. Engng*, **3**, 1.

HELLUMS, J. D. & CHURCHILL, S. W. 1961 Computation of natural convection by finite-difference methods. *A.S.M.E., Int. Develop. in Heat Transfer*, **5**, 984.

LARSON, D. W. 1972 Analytical study of heat transfer in an enclosure with flames. Ph.D. thesis, Purdue University.

NEWELL, M. E. & SCHMIDT, F. W. 1970 Heat transfer by laminar convection within rectangular enclosures. *J. Heat Transfer, Trans. A.S.M.E.* C**92**, 1959.

OZOE, H., SAYAMA, H. & CHURCHILL, S. W. 1974 Natural convection in inclined square channel. *Int. J. Heat Mass Transfer*, **17**, 401.

OZOE, H., SAYAMA, H. & CHURCHILL, S. W. 1975 Natural convection in an inclined rectangular channel at various aspect ratios and angles – experimental measurements. *Int. J. Heat Mass Transfer*, **18**, 1425.

OSTRACH, S. 1972 Natural convection in enclosures. *Adv. Heat Transfer*, **8**, 161.

PEACEMAN, D. W. & RACHFORD, H. H., 1955 The numerical solution of parabolic and elliptic difference equations. *J. S.I.A.M.* **3**, 28.

PECKOVER, R. S. & HUTCHINSON, I. S. 1974 Convective rolls driven by internal heat sources. *Phys. Fluids*, **17**, 1369.

ROACHE, P. J. 1972 *Computational Fluid Dynamics*. Albuquerque: Hermosa.

RUBEL, A. & LANDIS, F. 1969 Numerical study of natural convection in a vertical rectangular enclosure. *Phys. Fluids Suppl.* **12**, II 208.

SPARROW, E. M. & CESS, R. D. 1966 *Radiation Heat Transfer*. Belmont, California: Brooks/Cole Publishing.

TOOR, J. S. & VISKANTA, R. 1972 A critical examination of the validity of simplified models for radiant heat transfer analysis. *Int. J. Heat Mass Transfer*, **15**, 1553.

TORRANCE, K. E. 1968 Comparison of finite-difference computations of natural convection. *J. Res. Nat. Bur. Stand.* B**72**, 281.

TORRANCE, K. E., ORLOFF, L. & ROCKETT, J. A. 1969 Experiments on natural convection in enclosures with localized heating from below. *J. Fluid Mech.* **36**, 21.

TORRANCE, K. E. & ROCKETT, J. A. 1969 Numerical study of natural convection in an enclosure with localized heating from below: creeping flow to the onset of laminar instability. *J. Fluid Mech.* **36**, 33.

WILKES, J. O. & CHURCHILL, S. W. 1966 The finite-difference computation of natural convection in a rectangular enclosure. *A.I.Ch.E. J.* **12**, 161.